ARTICLE

Eliminating Capillary Coalescence of Nanowire Arrays with Applied Electric Fields

Justin J. Hill,[†] Kelly Haller,[†] Brittany Gelfand,[†] and Kirk J. Ziegler*[,†,‡]

Department of Chemical Engineering and Center for Surface Science and Engineering, University of Florida, Gainesville, Florida 32611

ABSTRACT Surface tension induces significant forces on wetted nanostructures, such as vertically oriented nanowire arrays, that can force them to aggregate when dried. This aggregation decreases the homogeneity and surface area of the array, often inhibiting their intended application. These aggregation forces are eliminated by introducing small electric fields (~100 V/m) during drying, providing a simple approach that is applicable to a broad range of nanowire materials, diameters, lengths, and spacing. A model based on the forces acting on two nanowires shows that electrostatic repulsion, rather than field-induced changes to the surface tension, provides the necessary forces to prevent aggregation. These calculations also highlight the substantial surface tension forces acting on nanostructures and the difficulties associated with preventing their aggregation.

KEYWORDS: nanowires • surface tension • capillary forces • aggregation • electric field

INTRODUCTION

Elasto-capillary coalescence of high-aspect-ratio structures is a phenomenon that has long existed in nature and artificial systems (1, 2). Chandra et al. studied this aggregation phenomena for hydrogel micropillars and found that the pillars clustered in predictably sized aggregates (3). Additionally, Pokroy et al. found there is a critical nanowire length that causes epoxy nanopillar arrays to undergo irreversible aggregation because of the short-range van der Waals forces (4). By tuning the nanopillar dimensions and separation distances, they were able to obtain complex and highly periodic chiral aggregates, which have potential applications in storing elastic energy, enhancing adhesion, or capturing and releasing particles (4).

Although the aggregation of high-aspect-ratio structures can be advantageous, this phenomenon is generally undesirable (5), especially in the fabrication of a high-density array of vertically oriented nanowires on a substrate (6−13). For example, when nanowires are deposited in porous templates, such as anodic aluminum oxide (AAO) (6−8) or self-assembled block copolymers (14), the template must often be removed with a liquid etchant to obtain a freestanding nanowire array (6−8, 14−16). When the array is composed of sufficiently high density and high-aspect-ratio nanowires, the surface tension between the residual fluid film and nanowires leads to aggregation.

The dynamics of nanowire aggregation induced by surface tension is quite complex. This process involves many factors, including the periodicity, dimensions, separation distance, and tensile strength of the nanowire, as well as the evaporation rate and the surface tension of the fluid. The tendency for the nanowires to aggregate during drying is sufficiently minimized only in the special cases where no fluid−solid meniscus is present, fluids with zero surface tension, or the obvious case where the nanowire is stiff enough to overcome the forces (4, 17). Currently, supercritical fluid drying (near zero surface tension fluid) is the only method that can inhibit the aggregation of nanowires by surface tension (17). Although critical point drying is an effective way to prevent aggregation, it is restricted to batch-type processes because of the high-pressure vessels. Therefore, this method has limited throughput and is energy-intensive.

In this paper, electric fields are used to minimize the aggregation of gold nanowire arrays during drying. Gold is electrochemically deposited in AAO templates, yielding arrays of nanowires with high surface energy (18) and low tensile strength. The voltage bias between the nanowire- and counter-electrode builds a capacitance layer on each nanowire, providing Coulombic repulsion while drying. The surface charge also alters the contact angle, as described by the Lippmann equation (19, 20). The nanowires were fabricated directly on tin-doped indium oxide (ITO) substrates (21) so that light transmission through the nanowire array could detect aggregation during the drying process. Experimental measurements and theoretical calculations show that small electric fields compensate for the aggregation force due to surface tension, providing a simple, scalable, and economical method to prepare nonaggregated arrays of high-density nanowires.

EXPERIMENTAL SECTION

Template Fabrication. Porous anodic aluminum oxide (AAO) templates were fabricated on transparent conductive substrates, composed of tin-doped indium oxide (ITO) on glass, as described elsewhere (21). Briefly, the ITO on glass was obtained precut from Thin Film Devices, Inc. with a film thickness of

* Corresponding author. E-mail: kziegler@che.ufl.edu.
Received for review March 31, 2010 and accepted June 28, 2010
[†] Department of Chemical Engineering, University of Florida.
[‡] Center for Surface Science and Engineering, University of Florida.
DOI: 10.1021/am100290z

Published on Web 07/12/2010

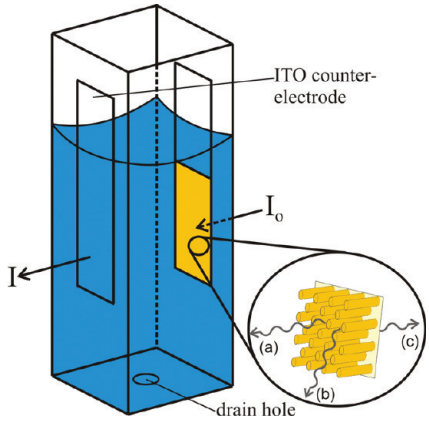

FIGURE 1. Custom-made view cell for monitoring the change in transmitted light through the gold nanowire arrays due to nanowire aggregation. The transparent and conductive ITO substrate positioned opposite of the nanowire substrate enables a variable electric field by either changing the working distance (*D*) or adjusting the applied bias (*V*) between the ITO and gold substrates. A drain hole removes the water and starts the nanowire drying process. The view cell is mounted on a rotational stage to ensure the incident light is parallel to nanowire orientation, maximizing the initial light transmittance. The light interacting with the nanowire array substrate can either (a) transmit, (b) scatter, (c) reflect, or be absorbed by the gold, ITO, glass, and water (not shown).

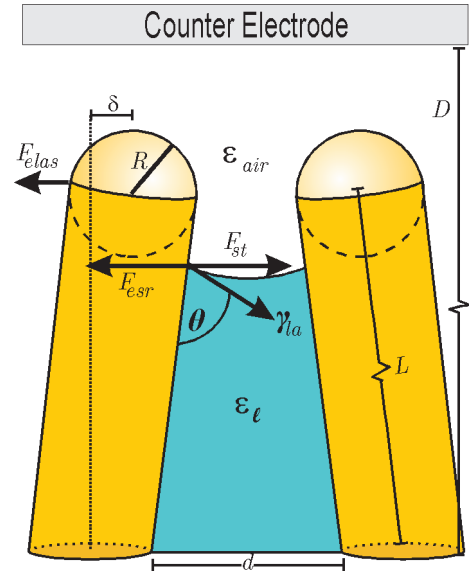

FIGURE 2. Schematic representation of the fundamental forces acting on a pair of wetted nanowires in the presence of an electric field. A meniscus forms when the fluid film dries below the tips of the nanowires. At this point, the force due to the surface tension (F_{st}) must be counter balanced by the elastic force of the bent nanowire (F_{elas}) and the electrostatic repulsive force (F_{esr}). The electrostatic force is due to the surface charge on the nanowires from the electric field, which is dependent on the field strength (V/D) and the dielectric constant of air (ε_{air}). The electrostatic repulsive force increases as the nanowires approach each other, providing enough force to eliminate aggregation under the proper conditions.

450 ± 15 nm and a sheet resistance <5 Ω/cm^2. Layers of chromium and aluminum (10 nm and 2.2 μm) were deposited at rates of 0.1 and 20 nm/s, respectively, using a custom electron-beam evaporation chamber operating at a pressure of 5×10^{-6} Torr. Following film deposition, aluminum anodization was carried out at constant voltage by increasing the potential at a rate of 100 V/min to a final voltage of 130 V using a Lambda Gen 300−5 power supply and a custom Labview control program. After complete anodization, the alumina barrier layer was etched with 5 wt % phosphoric acid for 330 s to expose the pore bottoms to the underlying ITO substrate.

Electrochemical Nanowire Synthesis. Gold nanowires were synthesized by electrochemically depositing gold from solution (Technigold 25 ES, Technic Inc.) onto the exposed ITO layer within the pores of the AAO template. The solution was held at 60 °C and deposition was performed potentiostatically (Versastat V3, Princeton Applied Research) against a carbon counter-electrode at −0.5 V referenced to a saturated calomel electrode. The deposition current was monitored closely so that gold deposition was ceased once the current began to rise dramatically, resulting in completely filled AAO template pores (22). The average diameter and length of the nanowires was 165 nm and 2.8 μm, respectively, and the average spacing between nanowires was 150 nm.

Immediately after deposition, the templated gold nanowires were rinsed with deionized water and then placed in 25 wt % phosphoric acid for 1−2 h to facilitate the selective removal of the alumina template. The freestanding array of vertical gold nanowires were removed from the acid solution, rinsed by immersion in deionized water and subsequently placed in fresh deionized water for storage. The nanowire arrays were stored in deionized water to prevent nanowire aggregation until further analysis was performed.

Nanowire Electrostatic Repulsion. Double-sided tape was used to attach the nanowire array substrate to a custom-built view cell filled with deionized water, as depicted in Figure 1. The array was quickly transferred to the view cell to minimize the exposure time to air before analysis; typically, it took less than 10 s to transfer the array. This apparatus was then mounted inside a spectrophotometer (Perkin-Elmer Lambda 9 UV/vis/NIR) for spectral analysis during film drying. Opposite of the nanowire array, a blank ITO substrate was positioned at variable working distances with the conductive side facing the nanowire surface, as shown in Figure 1. Electrodes were connected to both the blank ITO and the nanowire array substrate. A range of voltages (0 to 10 V) were applied with an Instek PSH 2018 power supply just after the fluid was drained from the view cell (within 5 s). Light transmittance data was collected at a wavelength of 550 nm once the fluid started draining until the substrate was completely dry. The extent of nanowire aggregation was also confirmed by field-emission scanning electron microscopy (JEOL JSM-6335F).

THEORY

Aggregation Due to Surface Tension. The aggregation of nanowire arrays due to surface tension arises from perturbations in the drying process, which can be intensified by inhomogeneities in nanowire sizes and spacing. Depending on the contact angle of the meniscus between two nanowires, either a repulsive or an attractive force can be exerted between them. If this force overwhelms the stiffness of the nanowire, then the nanowire will bend toward the other surrounding nanowires. This bending force can plastically deform the nanowire if the force is greater than the tensile strength of the material or push the nanowires close enough that surface energies or short-range van der Waals interactions keep them in contact (17, 23).

Neglecting the short-range van der Waals attractive forces between the nanowires, Figure 2 shows that a force balance describes the relation between the opposing forces from surface tension, F_{st}, the elastic bending force of the nanowire, F_{elas}, and any electrostatic repulsion, F_{esr}, from charge buildup on the nanowires

$$\sum F = F_{st} - F_{elas} - F_{esr} \quad (1)$$

If the sum of the forces is positive, then the nanowire bends until the forces balance, resulting in irreversible nanowire aggregation.

The force exerted between two nanowires by surface tension is related to the liquid−air surface tension, γ_{la}, by (3, 24)

$$F_{st} = 2\pi\gamma_{la}R^2\cos^2(\theta)\frac{1}{\sqrt{d(4R + d)}} \quad (2)$$

where R is the nanowire radius, d is the separation distance between nanowires, and θ is the meniscus contact angle (at zero applied field $\theta = \theta^o = 46°$).

The maximum bending torque occurs when the meniscus is at the top of the nanowire or the beginning of the drying process. The force required to bend the nanowire is

$$F_{elas} = \frac{3\pi ER^4\delta}{4L^3} \quad (3)$$

where E, L, and δ are Young's modulus, length, and deflection of the nanowire, respectively.

Equations 1−3 can be used to estimate the attractive or repulsive forces on the nanowires. In the absence of surface charge, i.e., $F_{esr} = 0$, and assuming Young's modulus of ~78 GPa, the gold nanowires fabricated in this study will have an aggregation force of approximately 1.3×10^{-8} N. Therefore, the nanowire−nanowire repulsive force due to surface charging must be on the order of at least 1×10^{-8} N to overcome the aggregation force from the surface tension of the fluid.

Electrostatic Repulsion. For two flat plate electrodes separated by a distance, D, in air with relative permittivity, ε_{air}, and an applied bias, V, between the two electrodes (see Figure 2), the capacitance, C, present on each electrode is given by the following two equations

$$C = \frac{Q}{V} \quad (4)$$

and

$$C = \varepsilon_o\varepsilon_{air}\frac{A_{fp}}{D} \quad (5)$$

where A_{fp} is the area of the flat plate counter electrode, ε_o is the permittivity of vacuum, and Q is the total charge on the electrode. The capacitance can increase substantially if one electrode has high surface roughness (25); however, a simple flat plate model is used because the separation distances used in this study are large relative to the roughness amplitude. Combining eqs 4 and 5 yields the relation between the total electric field, $\xi = V/D$, and the total charge density

$$\frac{Q}{A_{fp}} = \varepsilon_o\varepsilon_{air}\frac{V}{D} \quad (6)$$

Additionally, the Coulombic force between two discrete point charges of magnitude, q, and equal sign is given by

$$F_{Coul} = \frac{q^2}{4\pi\varepsilon_o\varepsilon_{air}|r|^2} \quad (7)$$

where r is the separation distance between the two points and q can be approximated as $q = (Q/A_{fp})A$, provided the charges are infinitely small. In writing the expression for q, A is the surface area of a spherical tip at the end of the nanowire and it is assumed that the charge collects at these spherical tips. Therefore, the total electrostatic repulsive force between two nanowires in close proximity to one another becomes:

$$F_{esr} = 4\pi\varepsilon_o\varepsilon_{air}\left(\frac{R^2}{d - 2\delta}\right)^2\left(\frac{V}{D}\right)^2 \quad (8)$$

As seen by eq 8, the electrostatic repulsive force becomes significant as the nanowires deflect toward each other.

Surface Tension Reduction. At constant electrochemical potential and temperature, the Lippmann Equation describes the changes in liquid−solid surface tension with respect to changing electric field, i.e., the liquid−solid surface tension changes as charge builds up on the nanowire surface (19, 20), which upon utilizing eq 6 becomes

$$\frac{\partial\gamma_{ls}}{\partial V} = -\frac{Q}{A} = -\varepsilon_o\varepsilon_{air}\frac{V}{D} \quad (9)$$

Integrating eq 9 and using the Young−Dupre equation yields (26)

$$\cos(\theta) = \cos(\theta^o) + \frac{\varepsilon_o\varepsilon_{air}}{2\gamma_{la}}\frac{V^2}{D} \quad (10)$$

which shows that the contact angle, θ, changes with the square of the applied voltage. The adjusted contact angle from eq 10 is inserted into eq 2 to yield a more complete expression for the force due to surface tension, showing that F_{st} scales with R and V^4.

Calculated Changes to Aggregation Behavior. Despite the fact that the forces modeled here for two nanowires do not include the network of multibody interactions found in actual nanowire arrays, the model illustrates the fundamental process and provides a guideline for preventing aggregation, as shown in Figure 3. Figure 3a outlines the dependence of nanowire length on the calculated forces

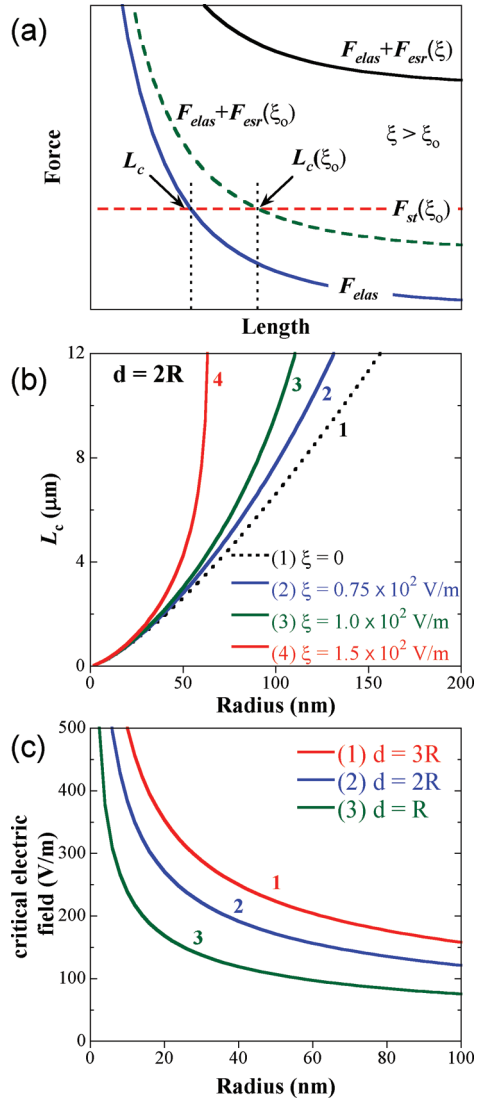

FIGURE 3. Calculated changes in aggregation behavior based on the forces acting on two nanowires. (a) The dependence of the surface tension force (F_{st}), elastic bending force (F_{elas}), and the overall repulsive force ($F_{elas} + F_{esr}$) as a function of nanowire length and electric field strength. The dotted lines are the forces at very low applied electric field and the solid lines represent the forces at higher electric fields, excluding the bending force, which is independent of applied field. The intersection of the repulsive force curves (either F_{elas} or $F_{elas} + F_{esr}$) with F_{st} designates the critical length, L_c, where the forces balance and a change in aggregation behavior occurs, i.e., maximum length before aggregation. Nanowire lengths longer than this point will aggregate. (b) The maximum length before aggregation, L_c, as a function of nanowire radius at a spacing of $d = 2R$. (c) The critical electric field required to prevent aggregation of nanowires of any length as a function of nanowire radius. Electric fields below the curves require nanowire lengths shorter than L_c to prevent aggregation.

involved in this two-body model. As seen in eq 1, the force due to surface tension, F_{st}, is the only attractive force. For a given R, this force is constant at any length, L. In the absence of an electric field, the only force countering F_{st} is the elastic bending force, F_{elas}. The intersection of these two curves in Figure 3a defines the critical nanowire length, L_c, where these forces balance. Nanowire lengths shorter than L_c have sufficient elastic energy to resist aggregation while those longer than L_c will aggregate. The application of a small electric field, ξ_o, provides additional electrostatic repulsive forces, F_{esr}, resulting in a new $L_c(\xi_o)$, as seen in Figure 3a; however, this small field has a minor influence on the aggregation behavior. Higher electric fields, ξ, provide substantial F_{esr}, raising the summed repulsive forces higher than F_{st}. At this field strength, nanowires of any length are forced apart, eliminating aggregation behavior due to surface tension. Although the field alters $F_{st}(\xi)$ through the Lippmann Equation, the effect is minimal (not shown).

The intersecting points between the curves for F_{st} and $F_{elas} + F_{esr}$ in Figure 3a can be plotted for a range of nanowire diameters and spacing to understand the overall effect of an applied electric field on aggregation behavior, as shown in Figure 3b. Without an electric field, the maximum length before the nanowires aggregate increases almost linearly as the nanowire radius becomes larger, as shown in Figure 3b for a constant ratio of nanowire spacing to radius. This reduction in aggregation behavior is because of the increased elastic bending force associated with stiffer nanowires. The application of an electric field provides additional repulsive interactions, indicating that a wider range of nanowire lengths will resist aggregation. The effect is minimal at small fields and radii but becomes more substantial with either larger fields or radii. Figure 3c describes the point where the F_{st} and $F_{elas} + F_{esr}$ curves in Figure 3a no longer intersect. This point defines the critical electric field where nanowires of any length will not aggregate. Small electric fields are required to prevent aggregation for nanowires with large radii; however, the required electric field increases with $R^{-0.5}$. This strong dependency on nanowire radius highlights the strong forces associated with surface tension in nanostructures.

These calculations show that an applied voltage of ~0.15 V between the nanowire- and counter-electrode in air, and electrode separation distances (D) on the order of a millimeter will completely overcome the force due to surface tension and prevent the aggregation of two nanowires with diameters similar to those fabricated in this study. However, this analysis considers only the forces between two lone nanowires and eliminates the multibody effect of the surrounding nanowires. These additional effects would reduce the net aggregation force, minimizing the required electric field and improving the range of lengths and diameters where the field will inhibit aggregation.

RESULTS AND DISCUSSION

Aggregation During Drying. The SEM images in Figure 4 show the extent of irreversible nanowire aggregation after removing the AAO template and drying the substrate. The top-down view in Figure 4a shows the aggregation of nanowires is quite severe and persistent throughout the substrate. Images b and c in Figure 4 show that nanowires remain attached to the substrate after drying. The average cluster of nanowires contains approximately 35 nanowires, which is highlighted in Figure 4b. The deflection length of individual nanowires depends on the nanowire density and can be as large as 750 nm, as shown in Figure 4b.

To obtain real-time analysis of the aggregation behavior, we fabricated the nanowires on transparent substrates so

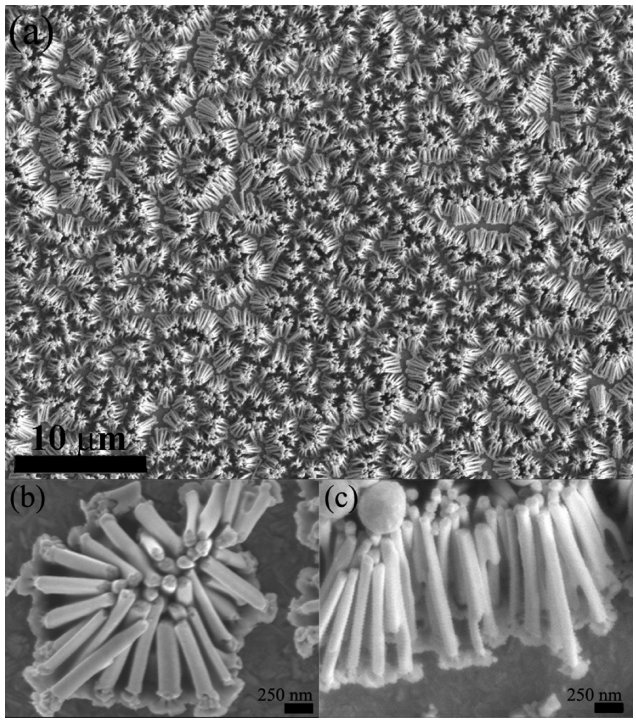

FIGURE 4. (a) SEM image of a gold nanowire array that dried normally, i.e., without an electric field present. Both (a, b) top-down and (c) side view images show the nanowires have undergone irreversible aggregation across the entire substrate. The HRSEM images (b, c) show that nanowires remain attached to the substrate and form well-defined clusters after drying.

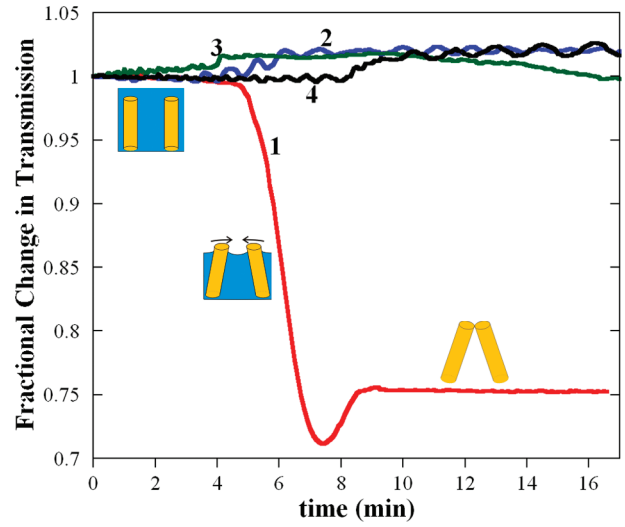

FIGURE 5. Fractional change in transmitted light (λ = 550 nm) through the nanowire arrays during drying for applied electric fields (ξ) of (1) 0, (2) 10^2, (3) 10^3, and (4) 10^4 V/m. When no field is applied, the transmission shows no changes, while the nanowires remain submerged under water (see cartoon). Once the water level falls below the tip of the nanowires, surface tension begins to deflect the nanowires toward each other. The final dried state is severely aggregated as indicated by the decrease in the transmittance. There is no decrease in transmission through the substrate in the presence of an electric field, indicating that minimal aggregation has occurred.

that light transmittance (%T) could be monitored as the nanowire array dried. The benefit is that the optical method probes a significant number of nanowire-nanowire interactions (estimated to be on the order of 1×10^{10} nanowires). As shown in Figure 1, the transmission of light through the nanowire array is affected by the absorption from gold, ITO, glass, and water; reflection from the film; or scattering. Therefore, any deflections in the position of the nanowires will influence light transmittance. Prior to draining the view cell depicted in Figure 1, we placed the substrate perpendicular to the incoming radiation and the transmitted light was maximized (usually to a value of about 60%T) by adjusting the cell orientation with a rotational stage. This was done to position the nanowires parallel to the incoming radiation.

Once the water is drained from the view cell and the fluid film on the array dries, nanowires begin to aggregate. The aggregation of the nanowires shown in Figure 4 alters light transmission through the nanowire array, as shown in Figure 5 for 2.8 μm long gold nanowires (curve 1). The nanowires are initially wetted and no change in transmission is observed as water begins to evaporate from the system. The transmittance then falls rapidly after 5 min. In this region, the water film has evaporated to the point where the water line is just below the top of the nanowires and the force due to surface tension is beginning to deflect the nanowires. As the nanowires bend toward each other, less light can pass through the nanowire array. Therefore, the fractional change in transmitted light is related to the nanowire aggregation density, whereas the slope of the transmittance curve is related to the rate of nanowire aggregation and the evaporation rate, which is a function of room temperature and humidity. The transmittance falls to a minimum value corresponding to the point of maximum nanowire aggregation. At this point, a small layer of water likely coats each nanowire. As this layer evaporates, the transmittance slightly increases to a plateau region that remains significantly below the initial transmittance. The SEM images in Figure 4 indicate that this permanent drop in transmittance is due to nanowire aggregation. Either the slight increase in transmittance from the minimum in Figure 5 could be due to a reduction in light absorption by water or by nanowire relaxation from the elastic force after surface tension is removed. The nanowires that remain aggregated after this relaxation are either plastically deformed or the bending force is balanced by van der Waals forces or the surface energy of the gold.

Electrostatic Repulsion. The drying process was also monitored spectroscopically with an applied electric field between the blank ITO substrate and nanowire array. The electric field could be adjusted by varying either the applied voltage or working distance (D). Figure 5 shows the transmittance while drying a 2.8 μm long gold nanowire array using a working distance of 1 mm and applied voltages of 0.1, 1, and 10 V, corresponding to electric field strengths of 1×10^2, 1×10^3, and 1×10^4 V/m, respectively. It is apparent that this range of electric fields eliminates the reduction in transmission observed with no applied bias, maintaining nearly constant light transmission throughout the drying process. The spectroscopic measurements suggest that all of the applied electric fields have inhibited nanowire aggregation. The SEM images in Figure 6 confirm

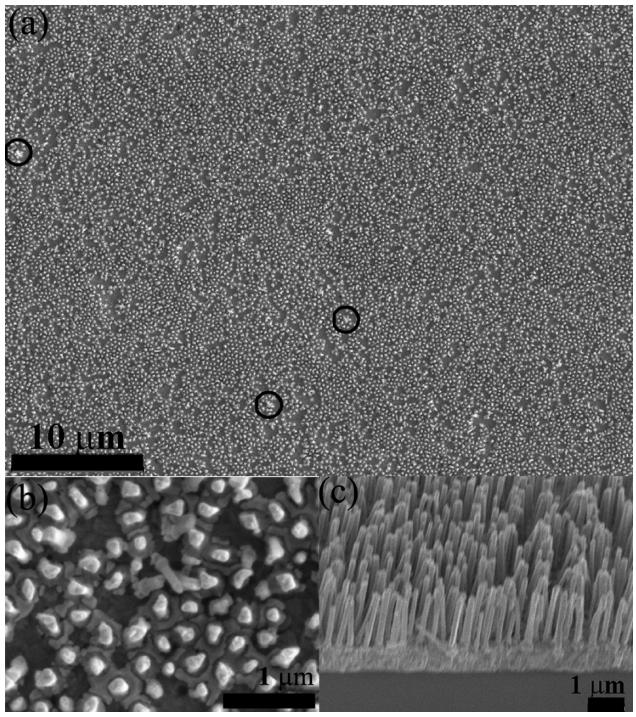

FIGURE 6. SEM image of a gold nanowire array that dried in the presence of a 10^4 V/m electric field. Both (a, b) top-down and (c) side view images show that the electric field diminishes nanowire aggregation. A few small aggregates of 2−5 nanowires can be observed in the substrate (circled in image). Note: the side view image (c) appears more aggregated than the top-down views (a, b) and could possibly be due to perturbations from breaking the film for image analysis.

that nanowire aggregation was diminished during the drying of each array. The images show that most of the nanowires are now oriented vertically. There are some areas of nanowire aggregation but these are limited to 2−5 nanowires and account for less than 5% of the substrate. Smaller electric fields were also used in an attempt to determine the critical electric field that prevents aggregation. However, fields as low as 1×10^{-1} V/m (the in situ experimental limitation) yielded inconsistent results, which could be due to differences in the fabrication of the nanowire arrays (e.g., diameters, lengths, and spacing).

The model results suggested that the 2.8 μm gold nanowires used in this study should not aggregate even without an electric field. Therefore, the model must underestimate the surface tension forces or overestimate the bending force. It should be noted that the model assumes the nanowire radius is uniform, whereas the nanowires fabricated for this study were purposely constructed to have a narrow neck at the base (see Figure 4b,c). This approach makes the arrays more susceptible to aggregation, enabling the study of the effect of the electric field, but makes comparisons to the model more difficult. If the bending force is based on nanowires with $(1/2)R$, then the model shows that 2.8 μm gold nanowires will aggregate. An electric field of $\sim 1 \times 10^2$ V/m would then provide enough electrostatic repulsion to prevent aggregation.

The use of electric fields provides a simple approach to prevent the aggregation of nanostructures. Although the nanowires could be transferred to other solvents to reduce the surface tension forces causing aggregation, these solvents still initiated complete aggregation of the nanowires (not shown). The only requirement of the electric field approach to preventing aggregation is that charge must build on the nanowire arrays. The material chosen for this study represents one of the more difficult systems to maintain as a vertical array. Therefore, it is likely that the method can be extended to other materials and substrates. The fields required to eliminate aggregation are also low enough to prevent damage to most nanostructured devices. The simplicity of the approach and equipment also allows the method to be easily scaled up, providing substantial benefits over critical point drying.

CONCLUSION

Electric fields as low as 1×10^2 V/m consistently inhibit the aggregation of gold nanowires when dried in water, providing a simple, generalized, and scalable approach to prevent the aggregation of nanowires on large-area substrates. The aggregation process can also be observed with optical transmission through the nanowire array. These results show that aggregation significantly decreases light transmission through the nanowire array. When electric fields are applied, only minor changes to the transmission are observed during the drying process, confirming that the nanowires always remain separated while drying. A simple model based on the forces acting on two nanowires showed that the dominant factor in eliminating aggregation is from electrostatic repulsion between the nanowires. The model also shows that aggregation in most typical nanowire arrays can be avoided with fields of $\sim 1 \times 10^2$ V/m. These results highlight the challenges associated with fabrication of high-density arrays of freestanding nanowires with small diameter.

Acknowledgment. Acknowledgment is made to the University of Florida Opportunity Fund for support of this research.

REFERENCES AND NOTES

(1) Boudaoud, A.; Bico, J.; Roman, B. *Phys. Rev. E* **2007**, *76*, 1–4.
(2) Bico, J.; Roman, B.; Moulin, L.; Boudaoud, A. *Nature* **2004**, *432*, 690–690.
(3) Chandra, D.; Yang, S.; Soshinsky, A.; Gambogi, R. *ACS Appl. Mater. Interfaces* **2009**, *1*, 1698–1704.
(4) Pokroy, B.; Kang, S. H.; Mahadevan, L.; Aizenberg, J. *Science* **2009**, *323*, 237–240.
(5) Dev, A.; Chaudhuri, S. *Nanotechnology* **2007**, *18*, 175607.
(6) Cao, G. Z. *J. Phys. Chem. B* **2004**, *108*, 19921–19931.
(7) Chu, S. Z.; Wada, K.; Inoue, S.; Todoroki, S. *Electrochim. Acta* **2003**, *48*, 3147–3153.
(8) Limmer, S. J.; Seraji, S.; Wu, Y.; Chou, T. P.; Nguyen, C.; Cao, G. Z. *Adv. Fun. Mater.* **2002**, *12*, 59–64.
(9) Petkov, N.; Platschek, B.; Morris, M. A.; Holmes, J. D.; Bein, T. *Chem. Mater.* **2007**, *19*, 1376–1381.
(10) Zhang, Q.; Li, Y.; Xu, D.; Gu, Z. *J. Mater. Sci. Lett.* **2001**, *20*, 925–937.
(11) Kim, H. C.; Jia, X.; Stafford, C. M.; Kim, D. H.; McCarthy, T. J.; Tuominen, M.; Hawker, C. J.; Russell, T. P. *Adv. Mater.* **2001**, *13*, 795–797.
(12) Lee, J. I.; Cho, S. H.; Park, S.-M.; Kim, J. K.; Kim, J. K.; Yu, J.-W.; Kim, Y. C.; Russell, T. P. *Nano Lett.* **2008**, *8*, 2315–2320.
(13) Park, S.; Kim, B.; Wang, J. Y.; Russell, T. P. *Adv. Mater.* **2008**, *20*, 681–685.

(14) Kim, J. U.; Cha, S. H.; Shin, K.; Jho, J. Y.; Lee, J. C. *Adv. Mater.* **2004**, *16*, 459–464.
(15) Chung, Y.; Lee, C.; Peng, C.; Chiu, H. *Mater. Chem. Phys.* **2006**, *100*, 380–384.
(16) Ishikawa, Y.; Matsumoto, Y. *Solid State Ionics* **2002**, *151*, 213–218.
(17) Liang, Y.; Zhen, C.; Zou, D.; Xu, D. *J. Am. Chem. Soc.* **2004**, *126*, 16338–16339.
(18) Diao, J.; Gall, K.; Dunn, M. L. *Phys. Rev. B* **2004**, *70*, 075413−1−075413−9.
(19) Lippmann, G. *Ann. Chim. Phys.* **1875**, *5*, 494–549.
(20) Newman, J.; Thomas-Alyea, K. E. *Electrochemical Systems*, 3rd ed.; Wiley-Interscience: Hoboken, NJ, 2004.
(21) Hill, J. J.; Haller, K.; Gelfand, B.; Ziegler, K. J. **2010**, submitted to *J. Electrochem. Soc.*
(22) Nasirpouri, F.; Southern, P.; Ghorbani, M.; Irajizad, A.; Schwarzacher, W. *J. Magn. Magn. Mater.* **2007**, *308*, 35–39.
(23) Ziegler, K. J.; Lyons, D. M.; Holmes, J. D. *Appl. Phys. Lett.* **2004**, *84*, 4074–4076.
(24) Kralchevsky, P. A.; Paunov, V. N.; Ivanov, I. B.; Nagayama, K. *J. Colloid Interface Sci.* **1992**, *151*, 79.
(25) Zhao, Y. P.; Wang, G. C.; Lu, T. M.; Palasantzas, G.; De Hosson, J. T. M. *Phys. Rev. B* **1999**, *60*, 9157.
(26) Nanayakkara, Y. S.; Moon, H.; Payagala, T.; Wijeratne, A. B.; Crank, J. A.; Sharma, P. S.; Armstrong, D. W. *Anal. Chem.* **2008**, *80*, 7690–7698.

AM100290Z